1999-01-5598

Advances in Projection Moiré Interferometry Development for Large Wind Tunnel Applications

Gary A. Fleming, Hector L. Soto, Bruce W. South, and Scott M. Bartram
NASA Langley Research Center

ABSTRACT

An instrument development program aimed at using Projection Moiré Interferometry (PMI) for acquiring model deformation measurements in large wind tunnels was begun at NASA Langley Research Center in 1996. Various improvements to the initial prototype PMI systems have been made throughout this development effort. This paper documents several of the most significant improvements to the optical hardware and image processing software, and addresses system implementation issues for large wind tunnel applications. The improvements have increased both measurement accuracy and instrument efficiency, promoting the routine use of PMI for model deformation measurements in production wind tunnel tests.

INTRODUCTION

Demands on wind tunnel instrumentation are continually increasing. It has been estimated that wind tunnel measurement accuracy requirements have increased by a factor of 10 over the past 10 years[1]. Additionally, significant reductions in test cycle time are needed to meet aerospace industry production goals. Thus new instruments developed for wind tunnel testing must not only be highly accurate, but also highly efficient.

Measurement of wind tunnel model deformation is critical to accurately assess vehicle drag and aeroelastic effects. Localized changes in angle-of-attack (AoA), such as wing twist, can significantly change the effective vehicle surface area, leading to errors in the computed drag coefficient (C_D). Considering C_D for many production wind tunnel tests must be measured to within $\pm$ 1 drag count, not compensating for model deformation can cause significant errors in the determination of this fundamental performance metric. Model deformation measurements are also essential when studying aeroelastic deformation. Progress in the development of compliant materials, actuators, and control mechanisms have now allowed aeroelasticity to be studied from an *enabling* viewpoint, examining how aeroelastic effects and deformable structures may be used to optimize aircraft configuration for a particular flight regime. Several aircraft manufacturers are currently conducting research on integrating smart materials and actuators into adaptive wing configurations[2-4]. Accurate model shape/deformation measurements during developmental wind tunnel tests are essential in understanding control surface actuation / aerodynamic reaction relationships.

An instrument development program aimed at using Projection Moiré Interferometry (PMI) for acquiring model deformation measurements in large wind tunnels was begun at NASA Langley Research Center (LaRC) in 1996. PMI is a video based, non-contacting instrumentation technique that can obtain spatially continuous model deformation measurements over the entire instrument field-of-view. Various improvements to the initial prototype PMI systems have been made throughout this development effort. This paper documents several of the most significant improvements to the optical hardware and image processing software, and addresses system implementation issues for large wind tunnel applications.

PROJECTION MOIRÉ INTERFEROMETRY (PMI)

PMI is an optically simple, non-contacting measurement technique used since the 1970s for surface topology and shape characterization[5]. The fundamentals of PMI are well known[6,7], but only recently have PMI and similar systems been used to quantitatively measure wind tunnel model deformations while under aerodynamic load[8-10]. The elegance of the technique is its optical simplicity, requiring only two major components: a projector and a video camera. The intricacies of the

technique lie within the image processing routines required to obtain quantitative deformation data.

PMI as applied to measuring wind tunnel model deformation is shown schematically in figure 1. A projection system is used to project a grid of equispaced, parallel lines onto the wind tunnel model surface. The projector system is typically aligned such that its optical axis is perpendicular to the surface being measured. A Ronchi ruling (a transmissive grating with opaque parallel lines etched at equal spacing and thickness) installed in the projector is the physical element generating the projected grid lines. A CCD camera with a narrow bandpass filter matched to the projector illumination wavelength is positioned to view the model at a 30-45 degree angle inclined from the projector optical axis. The projector and camera must lie within a plane perpendicular to the projected grid lines. Images of the grid lines projected onto the model are acquired in baseline (wind-off) and loaded (wind-on) conditions using a frame grabber installed in a PC -compatible computer. An example PMI raw data image is shown in figure 2. Image processing routines are then used to remove camera perspective distortion and interfere the acquired images with a computationally generated reference grid, resulting in interferograms containing moiré fringes, figure 3. These fringe patterns are further processed offline to obtain a quantitative, spatially continuous representation of the model surface shape or deformation[9], as shown in figure 4.

LARC PMI DEVELOPMENT EFFORT

The goal of the LaRC PMI development effort is to mature the PMI technique for the routine acquisition of spatially continuous, full-field model deformation measurements in production wind tunnels. Although other video photogrammetry-based model deformation measurement techniques have been used on a nearly routine basis in NASA facilities[11], PMI has the unique ability to provide *pictures* of model deformation, potentially representing the global deformation more accurately. The quantitative deformation measurement accuracy and resolution goals for PMI are 0.25- and 0.1-mm respectively, with ±0.025 degree localized twist measurement capability. These accuracy and resolution specifications are to be achieved for a 1.2-x 1.2-meter instrument field-of-view, typical of large wind tunnel applications.

Since the beginning of the LaRC PMI development effort, PMI systems have been used in the LaRC 14-by 22-Foot Subsonic Tunnel, Unitary Plan Wind Tunnel, and Transonic Dynamics Tunnel. The basic characteristics of these facilities are shown in Table 1. Deformation measurements of various models have been acquired at tunnel Mach numbers ranging from 0.1 to 2.2. Tests have been conducted in both air and R134a gas, for rotorcraft[9] and fixed-wing models[10]. Other LaRC tunnels where PMI may be used in the future include the National Transonic Facility and 16-Foot Transonic Tunnel. The e xtreme tunnel operating conditions must be considered when developing PMI instrumentation for these facilities.

Improvements to the initial prototype PMI system have been made throughout the development effort in pursuit of the accuracy and resolution goals, and to maximize instrument efficiency by:

1. Maximizing instrument ease of use
2. Minimizing cost per data point (including hardware costs, tunnel occupancy time for system installation and calibration, tunnel run time, and manpower)
3. Maximizing the ability of the instrument to convey results to the test engineer at rates sufficient to clearly and completely describe the global model deformation

Although the program development goals have not yet been achieved, the hardware/software/implementation enhancements described below have substantially improved the use of PMI for production wind tunnel testing.

PMI SYSTEM HARDWARE IMPROVEMENTS

PROJECTION SYSTEM ENHANCEMENTS

PMI projector systems can use any incoherent light source for grid line projection. For example, conventional slide projectors are often used in laboratory PMI systems. Unfortunately, commercially available slide, micromirror, or liquid crystal display-type units will not perform adequately for a for a majority of wind tunnel applications. These projectors are often too large to fit into wind tunnel optical access ports, and are not robust enough to withstand the temperature, pressure, and vibration extremes present in most tunnels. These projectors also do not provide the illumination necessary to acquire model deformation measurements in a lighted test section, or enough light intensity to acquire short exposure measurements.

All PMI projector systems constructed for use in LaRC wind tunnels employ broadband infrared (IR) laser diodes as the illumination source. Although laser illumination has the potential to cause speckle noise in the acquired PMI data images, diodes with 3 nm or greater emission linewidths are used to virtually eliminate this problem. The use of laser diodes provides numerous advantages over strobes, flashlamps, light emitting diodes, and other laser sources. Laser diodes provide the high output power needed for illumination of large areas, and, when used with appropriate receiving camera filters, allow for lights-on facility operation without loss of projected grid line contrast. Laser diodes also have small packaging and are very robust under harsh operating conditions. In addition to providing high

levels of continuous wave (CW) output power, laser diodes can be randomly pulsed to provide high intensity illumination for short time durations. This capability can be used to *freeze* the model position when excessive model dynamics are present, and to conditionally sample the model deformation.

Using diodes lasing in the near-IR allows PMI to be operated simultaneously with the wind tunnel optical measurement techniques shown in Table 2. By emitting at a discrete, isolated wavelength and using appropriate band-pass filters on receiving video cameras, the PMI system light can be isolated from light used by the other techniques. Thus tunnel run time can be minimized by acquiring PMI data while simultaneously acquiring other pressure, temperature, or flow velocity data.

The original prototype PMI system projector for wind tunnel use is shown in figure 5. Light emitting from a 15 Watt, 800 nm laser diode bar was collected by a 25-mm focal length cylindrical lens and directed to back-illuminate a Ronchi ruling. A conventional single-lens-reflex (SLR) camera lens was used to image the ruling and project the grid lines onto the test object. Although functional, this projector assembly was not optimal for wind tunnel applications. Aligning the discrete optical components in the confined space of a wind tunnel optical access port was difficult, as was obtaining optimal light throughput from the elliptically divergent laser diode. Additionally, the laser diode power supply was required to be within 2 meters of the laser. Significant line loss would occur over longer cable lengths, preventing the delivery of the 2.4 volt, 22 amps electrical power required to drive the laser diode. Implementing this projection system in most wind tunnels required installing the projector head and support electronics inside the tunnel test section. This subjected the electronics to the harsh tunnel environment, and prevented access to, and control of, the laser system during tests.

A fiber-coupled laser source and projector head assembly is now being implemented for grid line projection during wind tunnel tests. This new assembly, shown schematically in figure 6, allows the laser and power supply to reside in the tunnel control room where adjustments can be made during testing. Output light from the laser is transmitted via optical fiber to the projector head mounted in the tunnel test section. The fiber cable is an 800-micron, single core optical fiber, armour-coated to withstand the abusive wind tunnel environment. Cables consisting of fiber bundles were evaluated, but suffered from significant packing fraction losses and caused uneven, splotchy projector illumination patterns. Light exiting the single core fiber has a nearly uniform intensity distribution over 80% of the illumination diameter. Fiber lengths range from 25 to 35 meters, allowing installation of the projector head at virtually any location in or about the tunnel test section. The laser unit is capable of delivering up to 30 watts of 790 nm light at the fiber exit, enabling sufficient illumination of measurement areas up to twice as large as with the original prototype projector. The system can provide the same peak power in pulsed mode, allowing near-instantaneous deformation measurements of highly dynamic models. The unit can also output a single pulse of light in response to an external trigger, permitting the acquisition of conditionally sampled model deformation data.

Use of fiber-coupled laser light has significantly reduced the size and complexity of the projector head. The projector head is a 51 mm diameter cylindrical tube approximately 100 mm long, with a C-mount video lens attached for grid line projection. This geometry is small enough to allow for installation in virtually any wind tunnel optical access port. The optical fiber is attached to the rear of the projector head using a bulkhead connector compatible with the fiber termination. Light exiting the optical fiber diverges to back-illuminate a Ronchi ruling housed inside the projector head. The ruling position is adjusted to correspond with the image plane of the C-mount video lens, which projects the grid pattern onto the test object.

The new projector head design has greatly simplified the alignment process. The only alignment required is the adjustment of the ruling position to correspond with the projection lens image plane. This is accomplished by using a custom designed linear translation mechanism which moves the ruling axially along the length of the projector head tube. Adjustment of the ruling position can be performed while the projector head is fully assembled, eliminating the need to disassemble the projector head to reposition the ruling. Thus full alignment of the projector head can be accomplished within a few minutes, with minimal expertise.

Averting the discrete optics approach used in previous projector prototypes, figure 5, has increased the system robustness by minimizing possibility of misalignment caused by tunnel vibrations or flow buffeting. This robustness, however, can be compromised by the type of ruling installed in the projector head. Experience has shown that rulings with absorptive line patterns shatter under high laser power conditions, since at least 50 percent of the impinging light energy (i.e. up to 15 watts) is absorbed as heat. Rulings with reflective line patterns, such as evaporated chrome on glass, are highly recommended to avoid this problem.

IMAGING SYSTEM ENHANCEMENTS

Conventional RS-170 video cameras with 640-x 480-pixel resolution were used in early versions of LaRC PMI systems. The interlaced video stream generated by these cameras limited their usefulness for wind tunnel testing. Significant model dynamics and vibrations that are generally present during most wind tunnel tests can blur the projected grid lines during the 1/60 second CCD integration time. This problem was solved by electronically shuttering the camera to 0.1 ms, and pulsing the projection system laser only during the open

shutter period. This reduced the true camera resolution to 640-x 240-pixels since the projected grid pattern was visible to only one field of the interlaced video. Rows of the video fields captured as PMI data were interpolated to reconstruct a representative full resolution image. These images were processed independently, then averaged to determine the mean model deformation. Pulsed operation also reduced optical configuration flexibility since the projected grid lines needed to be observed perpendicular to the interlaced video rows. Otherwise, significant grid line aliasing could occur, to the point where the PMI system was non-functional.

The problems associated with RS-170 interlaced video cameras are being solved by implementing progressive scan cameras which integrate photons at each pixel simultaneously. Thus a non-interlaced, full-frame image can be obtained for each laser pulse. Progressive scan cameras with (a) high resolution CCD arrays and (b) IR optimized CCD arrays are currently being evaluated for use in LaRC PMI systems. The high resolution cameras, having 1300-x 1024-pixel resolution, have the potential to double the PMI system deformation measurement resolution compared to systems using 640-x 480-pixel cameras. The IR optimized cameras, although still having 640 -x 480-pixel arrays, have over twice the spectral sensitivity at 800 nm compared to their RS-170 counterparts. Thus the IR optimized cameras may prove critical for applications where surface scattered light is of low intensity, or when light collection is minimized by extremely short exposure times required for stop-motion images. Both progressive scan cameras have frame-on-demand (e.g. asynchronous reset) capability. This capability greatly simplifies conditional sampling of oscillating, rotating, or other highly dynamic model systems since the cameras can be triggered in response to an external event.

The imaging quality of the PMI receiver system must also be considered in addition to the practical operational characteristics of the camera. The PMI technique is highly dependent upon the ability of the imaging system to resolve the high spatial frequency intensity changes of the projected grid lines. Laboratory research has shown that grid line defocus constitutes one of the most significant imaging system-related error sources in PMI measurements[12]. Thus the receiver system must have good overall modulation transfer function characteristics to enable precise delineation of a grid line edge. The concept of *effective pixel resolution* is often used to quantify the imaging capability of an electronic imaging system, and is particularly useful when applied to PMI. The effective pixel resolution represents the number of actual pixels over which a sharp feature on the object would be blurred when imaged, and thus defines the minimum resolvable PMI projected grid line pitch. Both the imaging system camera and lens contribute to the effective pixel resolution. Within the camera, charge diffusion among adjacent pixel sites on the CCD array can lead to image blurring, causing a reduction in resolution. The effective pixel resolution can be further degraded by optical aberrations and distortions present in the lens.

The imaging system lens is a primary variable in PMI system optical configuration, chosen primarily to obtain the desired field-of-view. A variety of lens types, however, can be used to obtain similar adequate views. It was therefore necessary to evaluate several lens types to determine which, if any, produced the best effective pixel resolution when mated with a given camera. Thus a comprehensive effort was undertaken to examine the imaging system effective pixel resolution for a variety of off-the-shelf C-mount and SLR lenses used in LaRC PMI systems. A target with a black square was printed on a 600 dots-per-inch laser printer and illuminated using ambient room lighting. The target was imaged using a single RS-170 camera with eleven separate lenses including SLR, fixed focal length C-mount, high precision fixed-focal length C-mount, zoom, and telecentric video gauging lenses. Images of the target were digitized at 640-x 480-pixel resolution. All lenses were tested using f-number = 4, and relative image illumination and magnification were held constant by varying the room lighting intensity and camera-to-target distance. The imaging system edge spread function (ESF), shown in figure 7, was obtained for each lens by extracting value from a single row of pixels spanning the black/white target transition. The ESF was then differentiated to obtain the imaging system line spread function (LSF), figure 8. The full-width at half-maximum (FWHM) of the LSF was used to define the imaging system effective pixel resolution[13] listed in Table 3. The values listed in Table 3 show the effective pixel resolution was not significantly dependent upon the type of lens used, indicating the imaging system resolution limit was defined by the camera. The nominal effective resolution of 2 pixels also dictated the minimum resolvable PMI projected grid line pitch of 4 pixels per grid line. PMI systems used for wind tunnel testing at LaRC are typically configured for an observed projected grid line pitch of 6-8 pixels per grid line, well above the minimum resolution limit.

PMI SYSTEM SOFTWARE IMPROVEMENTS

Providing near real-time quantitative model deformation data is critical in establishing PMI as a viable tool for production wind tunnel testing. The present goal is to display a full-field, quantitative representation of the PMI-measured model deformation every three seconds. The current data processing rates must be reduced by a factor of 10 to achieve this goal.

Figure 2 illustrates the process of generating moiré fringes from the acquired PMI data images. After removal of perspective and optical distortions, the raw PMI image is interfered with a computationally generated reference grid. The reference grid is an image whose intensity varies sinusoidally across the rows at a spatial frequency equal to the projected grid line frequency

observed by the PMI system video camera. The interference process generates the low spatial frequency moiré fringes modulated by high spatial frequency artifacts of the projected grid lines. The interference process is performed four times, each with the computational reference grid phase incremented by 90 degrees. The high frequency artifacts must be filtered from each of the four phase stepped images to prevent their appearance as noise in the quantitative shape / deformation data. After filtering, the projected grid line phase distribution can be determined by[5]:

$$\theta = \tan^{-1}\left[\frac{I_{270} - I_{90}}{I_0 - I_{180}}\right] \qquad (1)$$

In equation (1) above, θ is the projected grid line phase, and I_x are the phase shifted interferograms as shown in figure 2, where the subscripts represent the phase of the computer generated reference grid. Equation (1) determines the grid line phase distribution modulo 2π, which must be unwrapped to remove the 2π discontinuities. The quantitative deformation profile is then determined by dividing the unwrapped phase distribution by the effective system wavenumber *k*, where:

$$k = \frac{2\pi}{Fringe\ Contour\ Interval} \qquad (2)$$

The fringe contour interval in equation (2) is the physical amount of deformation each fringe represents, determined by in-situ calibrations of the PMI system in the wind tunnel.

The process of filtering the high spatial frequency artifacts from moiré fringe images, figure 2, is computationally intensive and represents the greatest bottleneck in achieving near real-time performance. Filtering is currently accomplished by using a conventional 1-dimensional Fast Fourier Transform algorithm[14] applied to each row of the moiré fringe image. Results from the forward transform are multiplied by a low pass filter window to remove the high frequency artifacts. The resulting function is then inverse transformed to reconstruct the filtered moiré fringe image. This filtering process can take up to 6 seconds per phase shifted image when processed on a 400 MHz Pentium-class PC, far too slow for production wind tunnel use.

Several methods to accelerate the filtering process have been investigated, including wavelet filtering and the use of time optimized FFT routines. The wavelet filtering schemes tested did not exceed the previous FFT filtering capabilities in either processing time or filtering effectiveness, and thus were not pursued further. Instead, a variety of time optimized FFT routines were investigated for use in PMI filtering applications. The *FFTW* library of routines, developed at the Massachusetts Institute of Technology (MIT)[15], was tested for filtering performance on PMI moiré fringe images. These algorithms completed a filtering operation in *less than 1 second* when tested on a 400 MHz Pentium-class PC, providing a factor of 6 reduction in the time required for moiré fringe image filtering. The FFTW library will thus be used in all future versions of the LaRC PMI data processing software. These enhancements, coupled with additional procedures used to time optimize the PMI image processing code, are anticipated to reduce total processing times by a factor of 5 for 640-x 480-pixel images. This nears the 3-second data processing goal for production wind tunnel use, but image processing accelerator boards may be required for further reductions in data processing time.

PMI SYSTEM IMPLEMENTATION ISSUES

Research conducted during the LaRC PMI development program has resolved numerous issues regarding the use of PMI for model deformation measurements in wind tunnels. The hardware and software enhancements addressed above have solved many of the practical usage problems suffered by earlier prototype systems, and have lead to a generalized system design for wind tunnel use. These systems have been designed to acquire sequentially sampled measurements of static models, as well conditionally sampled measurements of rotating, oscillating, or fluttering bodies. As discussed in the *Productivity Enhancements* section below, several hardware features that were not available previously are now being exploited to increase instrument efficiency when conditionally sampled measurements are required.

Measurement quality, in addition to instrument usability, has also improved throughout the PMI development program. Tunnel testing experience has helped to identify various sources of PMI measurement error attributable to typical tunnel behavior, such as vibration and model dynamics. Procedural methods have been devised which minimize errors caused by these common tunnel characteristics. However, potential error sources caused by specific tunnel peculiarities must also be addressed. As shown in Table 1, the LaRC wind tunnels targeted for PMI use span a wide range of operating speeds, pressures, and temperatures. PMI systems used in these facilities would be calibrated in still air at STP after installation. Changes in the test media refractive index, caused either by temperature/pressure changes or physically changing the tunnel gas, could affect the PMI system measurement accuracy. Thus an investigation was conducted to quantify the potential magnitudes of this error source for the facilities listed in Table 1. This investigation is further described in the *Assessment of Refractive Index Effects* section below.

PRODUCTIVITY ENHANCEMENTS

The near-instantaneous, full-field measurement capability of PMI makes it an attractive method for

measuring deformations of oscillatory, rotating, or fluttering models. The PMI system can be externally triggered to acquire near-instantaneous data images in response to an external condition, allowing the detection of features that may otherwise be lost to time averaging. This capability is particularly useful when measuring rotorcraft blade bending and twist. Deformation measurements of rotorcraft blades must be acquired as a function of rotor azimuth since the blade attitude changes throughout the 360 degree revolution. Additionally, measurement of the rotation-to-rotation blade unsteadiness at a particular azimuth location is just as critical as the average blade deformation, since blade unsteadiness causes hub vibration and noise. The only way to measure both the mean and unsteady blade deformation is to acquire a set of near-instantaneous images of the blade, where each image in the set corresponds to another passage of the blade through the same azimuth location. The conditionally sampled data set may then be analyzed to quantitatively assess the mean and unsteady blade deformation.

Rotorcraft testing constitutes a significant portion of the tests conducted in the LaRC 14-by 22-Foot Subsonic Tunnel and Transonic Dynamics Tunnel. Although previous attempts at using PMI to measure the azimuthally dependent mean and unsteady rotor blade deformation were successful[9], the conditional sampling techniques employed were unacceptable for production wind tunnel use. The PMI video cameras used in these tests did not have asynchronous reset capability, and therefore could not be triggered when the rotor azimuth was at the designated measurement locations. Conditional sampling was performed by continuously capturing video and rotor azimuth position data at 10 Hz, and saving only the images acquired within 1.5 degrees of the desired azimuth locations. Although the PMI system was capable of 30 Hz video capture, the maximum 10 Hz sampling rate was dictated by the pulse rate of a Doppler Global Velocimeter used simultaneously during the test[16]. Acquiring azimuthally-dependent sets of PMI data in this manner required excessive amounts of tunnel run time. In some cases 20 minutes were required to capture enough images per azimuth location to constitute a statistically relavant data set.

A new conditional sampling scheme which exploits the asynchronous reset feature available on progressive scan CCD cameras is currently being developed for rotorcraft testing. A commercially available PC-plugin counter/timer board is used to monitor the rotor shaft position by counting pulses from a 1024 pulse/revolution encoder mounted on the rotor shaft. An encoder count (including a 1-2 count pretrigger delay) corresponding to an azimuth location where measurements are to be acquired is loaded into a comparator on the counter timer board. When the number of encoder pulses counted equals the value stored in the comparator, the counter/timer board triggers the camera, video frame grabber, and projection system laser. The laser system immediately pulses to illuminate the blades for 0.1 msec, essentially *freezing* the blade position and shape at the desired azimuth location. The video camera integration is gated to image the blade for the same 0.1 msec. The analog video data is then acquired by the frame grabber after the integration cycle, and subsequently stored to disk. The full implementation of this device will allow a single PMI data image to be captured at a designated azimuth location every other revolution, allowing 1 revolution for counter resetting and data transfer. Acquisition of a 50 image data set at a designated azimuth position can be completed within 5-10 seconds using this conditional sampling scheme. This represents a factor of 120 reduction in tunnel run time and cost to obtain such measurements compared to the conditional sampling methods used previously. This significant increase in instrument efficiency will allow PMI to be used for routine measurement of rotorcraft blade deformation during wind tunnel tests.

ASSESSMENT OF REFRACTIVE INDEX EFFECTS

An investigation was conducted to examine the extent of the errors caused by wind tunnel media refractive index changes on PMI measurement accuracy. This error source was of particular concern for the National Transonic Facility (NTF) and Transonic Dynamics Tunnel (TDT), as these tunnels often use test media other than air. The NTF uses cryogenic nitrogen to increase Reynolds number capability, and the TDT uses R134a gas to increase Reynolds number and achieve proper aeroelastic scaling. Figures 9-11 show the calculated refractive index, n , of 800 nm light for dry air, diatomic nitrogen, and R134a gas for a static pressure and static temperature range covering most tunnel operating conditions. The refractive index curves shown in figures 9-11 were computed using the empirical relation[17]:

$$r = \frac{r_0 P}{(1 + \alpha t)}; \quad r = (n-1)\times 10^6 \qquad (3)$$

where P is the gas static pressure in atmospheres, t is the gas static temperature in °C, $\alpha = 1/273$, and r_0 is the value of r computed for the gas refractive index at 0 °C, 1 atmosphere pressure. Values of r_0 for dry air, nitrogen, and R134a are 288.67, 297.49, and 714.00 respectively. Data describing the refractive index characteristics of R134a could not be found, so the r_0 value for R134a has been estimated using refractive index data of similar refrigerant gases. The refractive index pressure/temperature dependence of R134a has also been assumed to be the same as dry air. Real gas effects have been neglected in this analysis.

An optical ray tracing program was used to assess the effects of the refractive index changes shown in figures 9-11 on PMI system measurement accuracy. Two models simulating PMI system use in wind tunnels were

created. The first model, shown in figure 12, simulated a PMI installation in facilities where the optics would be located outside the tunnel test section viewing the model through a 25 mm thick quartz window. This emulates PMI system use in the NTF, Unitary Plan Wind Tunnel, and 16-Foot Transonic Tunnel. A second model was generated simulating PMI installations in the TDT and 14-by 22-Foot Subsonic Tunnel, where the optics are installed directly in the test section and are immersed in the test media. PMI systems used in these facilities do not view the model through a window. Although test media refractive index changes can impart several errors on PMI measurements, the most significant is the change in the projected grid line pitch as observed by the PMI video camera. This effect was evaluated by changing the test media refractive index in the ray trace models, and examining the corresponding change in grid line pitch calculated by the ray trace program. An indication of the resulting PMI system measurement error was obtained by computing the change in grid line pitch relative to that observed in air at STP (PMI system calibration conditions).

Table 4 shows the calculated worst case PMI measurement error caused by refractive index changes in the facilities targeted for PMI use. The tunnel conditions where the maximum error occurs are also listed. The errors caused by refractive index changes are negligible in all facilities with exception of the NTF operating with cryogenic nitrogen as the test media. In this case, refractive index changes may cause errors as large as 0.27 percent within PMI data acquired at the tunnel minimum temperature / maximum pressure extremes. Although this error source may be significant for some applications, other error sources that emerge with changing tunnel condition will likely dominate the PMI error budget in the NTF. More importantly, however, this analysis has indicated that refractive index errors in NTF should not be greater than 0.3 percent, and has eliminated refractive index as a significant error source in the other facilities.

CONCLUDING REMARKS

This paper documents progress in the LaRC PMI development effort to establish PMI as a viable tool for model deformation measurement in production wind tunnel tests. Measurement accuracy, as well as instrument efficiency, has been emphasized throughout the development program.

The error analyses and performance studies presented have aided in identifying which error sources are most significant for PMI use in wind tunnels. Computational investigations have been used to eliminate bulk refractive index changes in the wind tunnel test media as a significant error source in most facilities. These investigations have also revealed that refractive index effects may be significant in the National Transonic Facility, but should not affect PMI measurements by more than 0.3 percent.

Experiments conducted to examine the effect of receiver lens type on the PMI imaging system performance have also been presented. The results of the study showed that the imaging system effective pixel resolution was independent of the type of lens used, and was thus defined by the camera. The imaging system effective pixel resolution was found to be 2 pixels, dictating a minimum resolvable projected grid line pitch of 4 pixels per grid line. This metric is now used as a system design criteria when configuring PMI systems for wind tunnel use.

The PMI system hardware and software enhancements addressed in this paper have significantly increased instrument efficiency by maximizing the instrument ease of use and minimizing the cost per data point. The use of fiber-coupled laser diodes as projector illumination source has greatly simplified PMI system implementation in wind tunnels, and allows full system control during wind tunnel tests. Software routines with the potential to reduce data processing time by a factor of 5 are being incorporated to achieve near real-time data turnaround. New conditional sampling methods are being developed that can reduce PMI data acquisition time by a factor of 120 in rotorcraft applications, drastically reducing the tunnel run time and cost required to obtain blade deformation measurements.

Future PMI system enhancements planned include the development of advanced calibration procedures, and fully automated data acquisition controlled by the tunnel data acquisition system. Measurement uncertainty analyses and accuracy studies will also continue. Although additional PMI development is required to fully meet the development program objectives, the advances described in this paper have greatly promoted the routine use of PMI for model deformation measurements in production wind tunnels.

REFERENCES

1. Kegelman, J.T., “Recent Cycle Time Reduction at Langley Research Center”, AIAA-99-0178, presented at the 37th AIAA Aerospace Sciences Meeting and Exhibit, Reno, Nevada, January 11-14, 1999.
2. Kudva, J. N. et al., “Overview of the DARPA/AFRL/NASA Smart Wing Program”, Paper No. 3674-26, presented at the SPIE Symposium on Smart Structures and Materials, SPIE Vol. 3674, Newport Beach, CA, March 1-4, 1999.
3. Hall, J. M., “Executive Summary AFTI/F-111 Mission Adaptive Wing”, WRDC-TR-89-3083, September 1989.
4. Pendelton, E., et al., “A Flight Research Program for Active Aeroelastic Wing Technology”, AIAA Paper 96-1574, presented at the 37th AIAA SDM Conference, Salt Lake City, UT, April 15-17, 1996.

5. Patorski, K., Handbook of the Moiré Fringe Technique, Elsevier Science Publishers, 1993. pp. vii – xi, pp. 372-373.

6. Pirodda, L., "Shadow and projection moiré techniques for absolute or relative mapping of surface shapes", Optical Engineering 21(4), pp. 640-649, July/August 1982.

7. Selected Papers on Optical Moiré and Applications, SPIE Milestone Series, Vol. MS 64, 1992. Indebetouw, G., and Czarnek, R., editors.

8. Mercker, E., Pengel, K., Kube, R., Van der Wall, B., Boutier, A., Micheli, F., "On the Blade Deformation Measured at a Scaled Helicopter Rotor", Proceedings on Aeromechanics Technology and Product Design, Bridgeport, CT, October 11-13, 1995.

9. Fleming, G. A., and Gorton, S. A., "Measurement of Rotorcraft Blade Deformation using Projection Moiré Interferometry", Presented at the Third International Conference on Vibration Measurements by Laser Techniques, Ancona, Italy, June 16-19, 1998. SPIE Vol. 3411, pp. 514-527.

10. Fleming, G. A., and Burner, A. W., "Deformation measurements of smart aerodynamic surfaces", SPIE Paper No. 3783-25, Presented at the 44th Annual SPIE International Symposium on Optical Science, Engineering, and Instrumentation - Optical Diagnostics for Fluids/Heat/Combustion and Photomechanics for Solids, Denver, CO, 18-23 July 1999.

11. A. W. Burner, Model Deformation Measurements at NASA Langley Research Center, AGARD 81st Fluid Dynamics Panel Symposium on Advanced Aerodynamic Measurement Technology, Seattle, Washington, September 22-25, 1997.

12. Pryputniewicz, E. J., *Development of PMI Systems for Characterization of Load-Resisting Structures*, Major Qualifying Project, Worcester Polytechnic Institute, Worcester, MA, 1999.

13. Handbook of Optics, Volume II – Devices, Measurements, and Properties, 2nd Edition. M. Bass, editor. McGraw-Hill, Inc. New York, 1995, pp. 11.6 .

14. Press, W. H., Teukolsky, S. A., Vetterling, W. T., and Flannery, B. P., Numerical Recipes in Fortran, 2nd Edition. Cambridge University Press, 1992, pp. 490.

15. Frigo, M., and Johnson, S. G., "FFTW: An Adaptive Software Architecture for the FFT", Proceedings of the International Conference on Acoustics, Speech, and Signal Processing, Seattle, WA, May 12-15, 1998. Vol. 3, pp. 1381.

16. Meyers, J. F., Fleming, G. A., Gorton, S. A., and Berry, J. D., "Instantaneous Doppler Global Velocimetry Measurements of a Rotor Wake: Lessons Learned", Presented at the 9th International Symposium on Applications of Laser Techniques to Fluid Mechanics, Lisbon, Portugal. July 13-16, 1998.

17. Fox, J. J., and Tate, F. G. H., "Refractivity of all gases and vapors and of elementary substances in the isotropic solid and liquid states", in the International Critical Tables of Numerical Data – Physics, Chemistry, and Technology, Volume VII – 1st Edition. McGraw-Hill, Inc., New York, 1930.

Table 1: Candidate facilities for PMI use at NASA Langley Research Center

Facility	Test section size, w-x h, meters	Media	Max. Mach #	Static Pressure, atm	Static Temp., °C
14-by 22-Foot Subsonic Tunnel	6.7-x 4.3	Air	0.3	1.0	10 – 37
Unitary Plan Wind Tunnel	1.2-x 1.2	Air	4.6	0.0 – 3.0	15 – 45
Transonic Dynamics Tunnel	4.9-x 4.9	Air, R134a	1.2	0.0 – 1.0	25 – 50
16-Foot Transonic Tunnel	4.9-m dia.	Air	1.2	0.3 – 1.0	5 – 140
National Transonic Facility	2.5-x 2.5	Air	1.2	0.5 – 4.0	25 – 50
National Transonic Facility	2.5-x 2.5	Nitrogen	1.2	0.5 – 4.0	-150 – 50

Table 2: Optical measurement techniques used in wind tunnel applications

Measurement Technique	Measurand	Typical Operating Wavelength(s), nm
Projection Moiré Interferometry	Model Deformation	800
Video Photogrammetry	Model Deformation	Visible
Laser Velocimetry (fringe type)	Off-body velocity, single point	476, 488, 514
Doppler Global Velocimetry	Off-body velocity, planar	514, 532
Particle Image Velocimetry	Off-body velocity, planar	532
Pressure/Temperature Sensitive Paint	On-body pressure/temperature	400 ± 50, 650 ± 50
Laser Induced Thermal Acoustics	Simultaneous temperature, density, speed of sound	532, 750, 1064
IR Thermography	Transition detection	4000 ± 1000
Phosphor Thermography	Aerothermal heating	365, 600 ± 50

Table 3: PMI receiver system effective pixel resolution for various lens types

Lens Type	Effective Resolution, pixels
SLR, f = 35 mm	1.93
SLR, f = 50 mm	1.98
C-mount, f = 12.5 – 75 mm zoom, f = 12.5 mm	2.02
C-mount, f = 12.5 – 75 mm zoom, f = 75 mm	2.02
C-mount, f = 25 mm	1.87
C-mount, f = 35 mm	1.99
C-mount, f = 50 mm	1.87
C-mount, f = 75 mm	1.89
C-mount, f = 75 mm television camera lens	2.02
C-mount, f = 17 mm high precision lens	1.91
C-mount, f = 35 mm high precision lens	2.02
C-mount, f = 55 mm telecentric gauging lens	1.93

Table 4: Calculated PMI system measurement errors caused by changes in the wind tunnel test medi refractive index

Facility	Maximum PMI Measurement Error, %	Tunnel Operating Condition	
		P_{stat}, atm	T_{stat}, °C
14-by 22-Foot Subsonic Tunnel	< 0.01	NA	NA
Unitary Plan Wind Tunnel	+ 0.03	Near vaccuum	15
Transonic Dynamics Tunnel, media = air	- 0.06	Near vaccuum	25
Transonic Dynamics Tunnel, media = R134a	+ 0.09	1	25
16-Foot Transonic Tunnel	+ 0.02	0.3	140
National Transonic Facility, media = air	- 0.09	4	25
National Transonic Facility, media = nitrogen	- 0.27	4	- 150

Figure 1: Conceptual use of PMI for wind tunnel model deformation measurements

Figure 2: Raw PMI data image showing projected grid lines

Figure 3: Moiré fringes generated by interfering PMI projected grid lines, figure 2, with a computationally generated reference grid

Figure 4: PMI-measured airfoil shape data obtained by processing moiré fringe images as in figure 3

Figure 5: Original prototype laser diode-based PMI projection system

Figure 6: Schematic of fiber-optically coupled PMI projector system and projector head

Figure 7: Typical PMI receiver system edge spread function (ESF)

Figure 8: Typical PMI imaging system line spread function, obtained by differentiating the ESF in figure 7.

Figure 9: Calculated refractive index behavior of 800 nm light in dry air

Figure 10: Calculated refractive index behavior of 800 nm light in nitrogen

Figure 11: Calculated refractive index behavior of 800 nm light in R134a gas

Figure 12: Optical ray trace model used to study refractive index effects on PMI system measurement accuracy

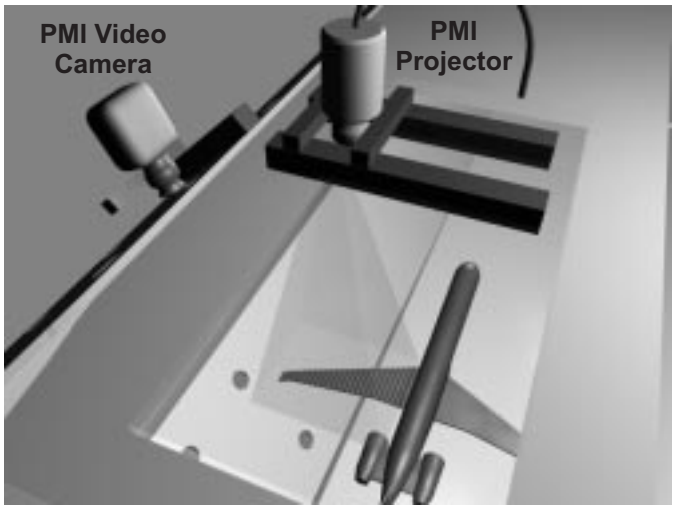

Figure 1: Conceptual use of PMI for wind tunnel model deformation measurements

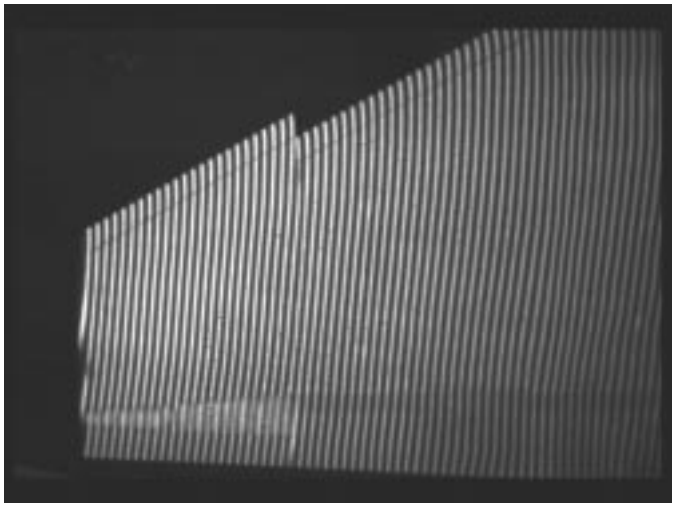

Figure 2: Raw PMI data image showing projected grid lines

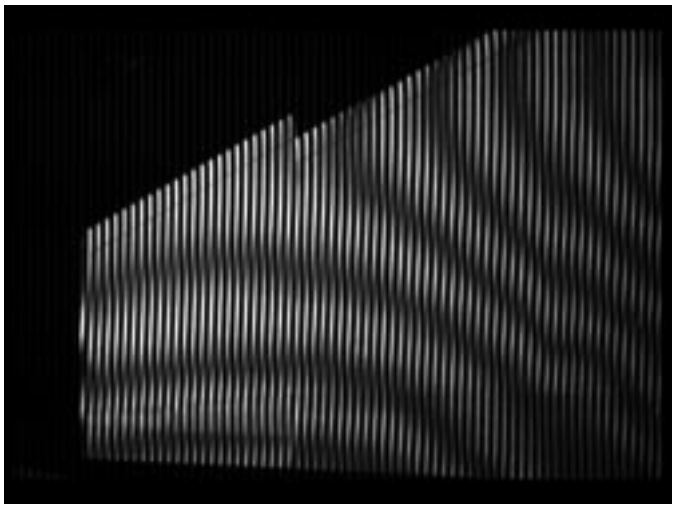

Figure 3: Moiré fringes generated by interfering PMI projected grid lines, figure 2, with a computationally generated reference grid

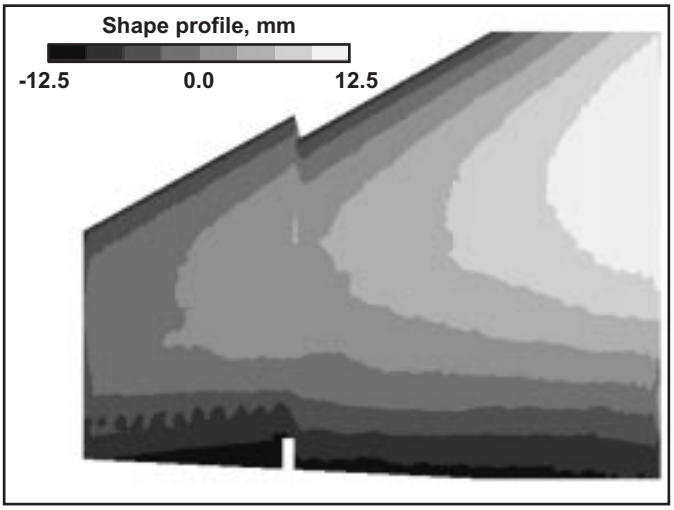

Figure 4: PMI-measured airfoil shape data obtained by processing moiré fringe images as in figure 3

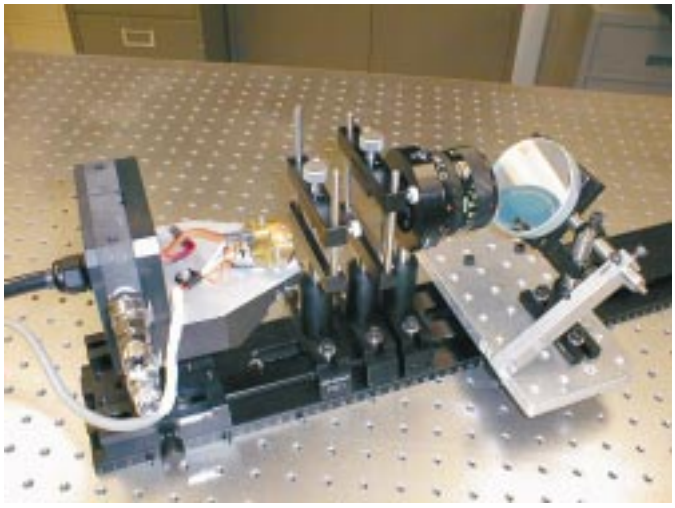

Figure 5: Original prototype laser diode-based PMI projection system

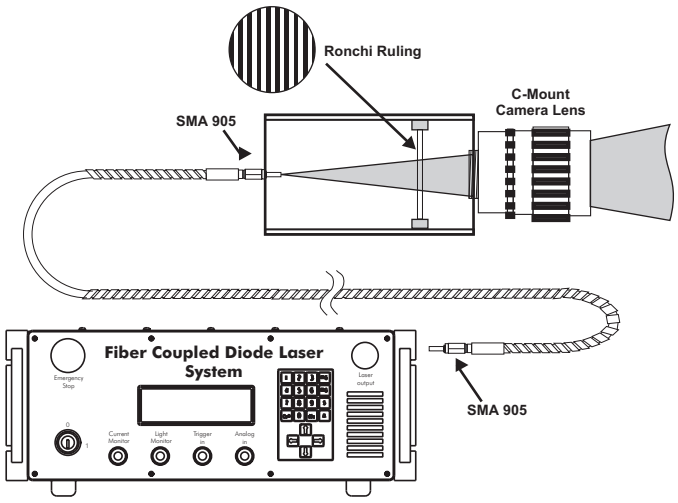

Figure 6: Schematic of fiber-optically coupled PMI projector system and projector head

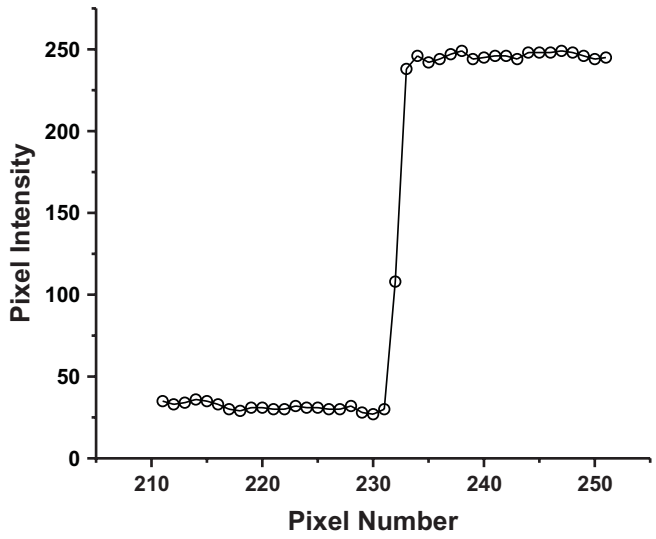

Figure 7: Typical PMI receiver system edge spread function (ESF)

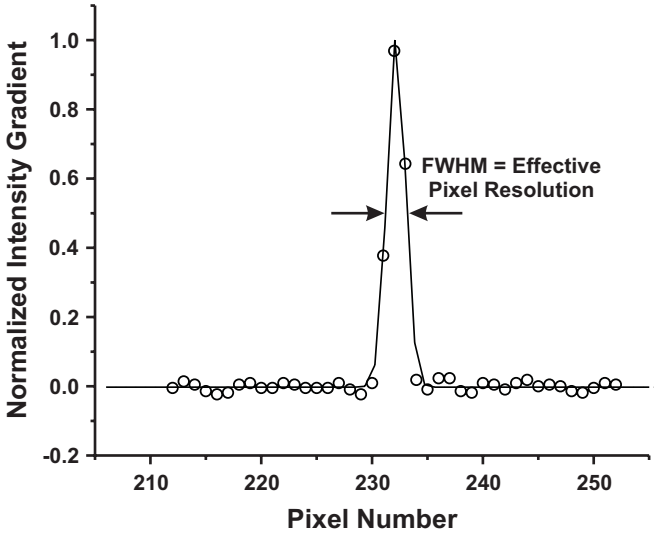

Figure 8: Typical PMI imaging system line spread function, obtained by differentiating the ESF in figure 7.

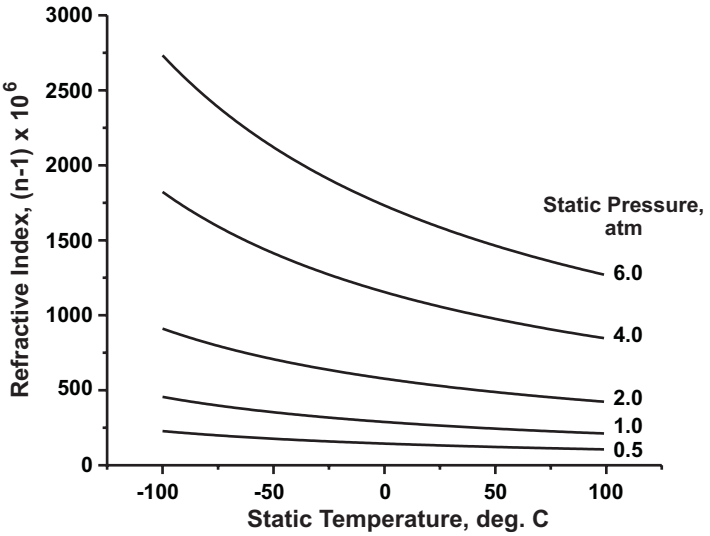

Figure 9: Calculated refractive index behavior of 800 nm light in dry air

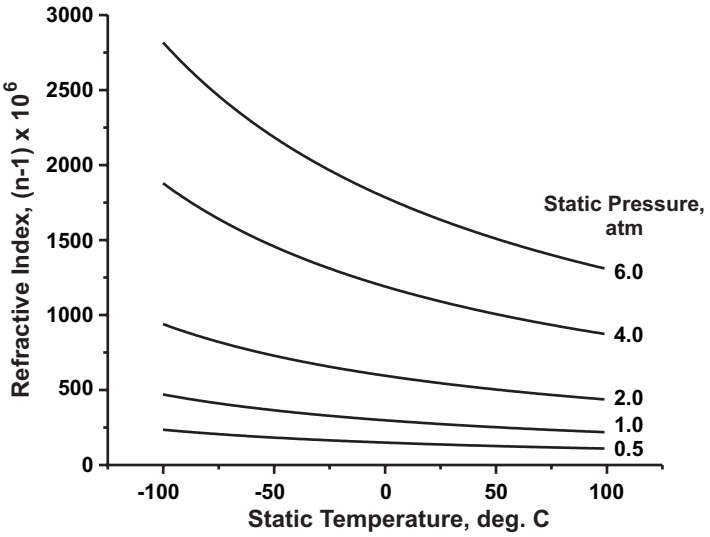

Figure 10: Calculated refractive index behavior of 800 nm light in nitrogen

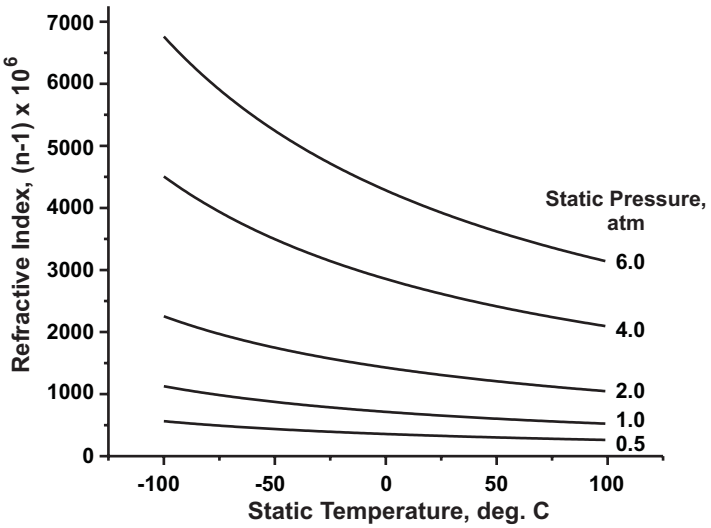

Figure 11: Calculated refractive index behavior of 800 nm light in R134a gas

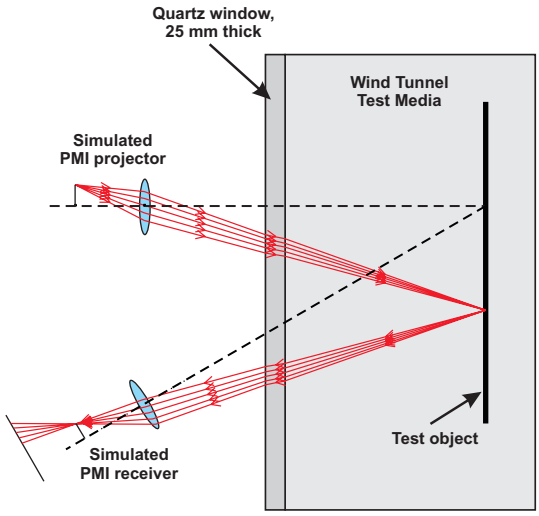

Figure 12: Optical ray trace model used to study refractive index effects on PMI system measurement accuracy